

# The spatial heterogeneity of cloud phase observed by satellite

Adam B Sokol<sup>1</sup> and Trude Storelvmo<sup>2</sup>

<sup>1</sup>University of Washington

<sup>2</sup>University of Oslo

November 23, 2022

## Abstract

We conduct a global assessment of the spatial heterogeneity of cloud phase within the temperature range where liquid and ice can coexist. Single-shot CALIOP lidar retrievals are used to examine cloud phase at the 333-m scale, and heterogeneity is quantified according to the frequency of switches between liquid and ice along the satellite's path. In the global mean, heterogeneity is greatest from -15 to -2C with a peak at -4C, when small patches of ice are prevalent within liquid-dominated clouds. Above -20C, heterogeneity is greatest in the northern midlatitudes and lower over the Southern Ocean, where supercooled liquid clouds dominate. Zonal mean heterogeneity undergoes an annual cycle with a peak that follows seasonal shifts in the extratropical storm track. These results can be used to improve the representation of subgrid-scale heterogeneity in general circulation models, which has the potential to reduce model biases in phase partitioning and radiation balance.

1     **The spatial heterogeneity of cloud phase observed by**  
2                     **satellite**

3                     **Adam B. Sokol<sup>1</sup>, Trude Storelvmo<sup>2</sup>**

4                     <sup>1</sup>Department of Atmospheric Sciences, University of Washington, Seattle, WA, USA

5                     <sup>2</sup>Department of Geosciences, University of Oslo, Oslo, Norway,

6                     **Key Points:**

- 7                     • Cloud phase heterogeneity observed by lidar is greatest a few degrees below freez-  
8                     ing, when single-phase patches are 6 km in length on average
- 9                     • Heterogeneity is greatest in the northern mid-latitudes and relatively low over the  
10                    Southern Ocean
- 11                    • Extratropical heterogeneity undergoes an annual cycle that reflects seasonal shifts  
12                    in the storm track

**Abstract**

We conduct a global assessment of the spatial heterogeneity of cloud phase within the temperature range where liquid and ice can coexist. Single-shot CALIOP lidar retrievals are used to examine cloud phase at the 333-m scale, and heterogeneity is quantified according to the frequency of switches between liquid and ice along the satellite's path. In the global mean, heterogeneity is greatest from -15 to -2°C with a peak at -4°C, when small patches of ice are prevalent within liquid-dominated clouds. Above -20°C, heterogeneity is greatest in the northern midlatitudes and lower over the Southern Ocean, where supercooled liquid clouds dominate. Zonal mean heterogeneity undergoes an annual cycle with a peak that follows seasonal shifts in the extratropical storm track. These results can be used to improve the representation of subgrid-scale heterogeneity in general circulation models, which has the potential to reduce model biases in phase partitioning and radiation balance.

**Plain Language Summary**

At temperatures where ice and liquid can coexist within clouds, climate models produce too much ice and too little liquid compared to satellite observations. This bias is caused by the assumption that liquid and ice are uniformly mixed, which results in the rapid conversion of liquid to ice for thermodynamic reasons. To reduce this bias, models need to account for the spatial heterogeneity (“patchiness”) of liquid and ice that exists in the real atmosphere. The goal of this paper is to quantify this spatial heterogeneity using satellite observations of cloud phase. To do so, we use vertical profiles of cloud phase observed by the CALIOP lidar every 333 m along the satellite's path. Clouds with small alternating pockets of liquid and ice are said to be more heterogeneous. We find small pockets of ice in liquid-dominated clouds to be more common than small pockets of liquid in ice-dominated clouds. The greatest heterogeneity is found in the northern midlatitudes and follows seasonal shifts in storminess. Phase is relatively homogeneous over the Southern Ocean, where supercooled liquid clouds dominate. These results can be used in the future to improve model representations of the thermodynamic processes responsible for biases in cloud phase.

## 1 Introduction

Cloud feedbacks remain a leading source of uncertainty in estimates of climate sensitivity (Zelinka et al., 2020). One such feedback is the cloud phase feedback, which was first described by Mitchell et al. (1989) as a negative feedback resulting from a shift in cloud phase partitioning from ice to liquid with warming. The feedback is negative because liquid cloud droplets are generally smaller and more numerous than ice crystals, which means that liquid clouds are optically thicker than ice clouds of equal condensate mass. A shift in phase partitioning from ice to liquid therefore produces an increase in cloud albedo.

The magnitude of the cloud phase feedback has proved tricky to constrain using models, largely because of its sensitivity to the phase partitioning of the initial state (Storelvmo et al., 2015; Choi et al., 2014; Tsushima et al., 2006). General circulation models (GCMs) systematically produce too much ice and too little liquid within the mixed-phase temperature range ( $-40$  to  $0^\circ$ ), especially over the Southern Ocean (Cesana et al., 2015; Komurcu et al., 2014; Kay et al., 2016). As a result, present-day cloud albedo is too low in many GCM simulations, and the albedo enhancement associated with ice-to-liquid transitions is too dramatic. Adjustment of present-day phase partitioning to more closely match observations results in a weakened cloud phase feedback and an increase in simulated climate sensitivity (Tan et al., 2016; Frey & Kay, 2018)

Model biases in phase partitioning are thought to be caused, at least in part, by an overactive Wegener-Bergeron-Findeisen (WBF) process (Tan & Storelvmo, 2016; McIlhatten et al., 2017). The WBF process is a consequence of the difference in saturation vapor pressures with respect to liquid and ice, which, in a mixed-phase environment, can cause ice crystals to grow at the expense of nearby liquid droplets (Storelvmo & Tan, 2015). GCM parameterizations of the WBF process typically assume that liquid and ice are homogeneously mixed throughout a model grid box, which allows for efficient WBF glaciation of supercooled liquid. But aircraft observations, while limited, suggest that mixed-phase clouds often contain discrete liquid-only and ice-only pockets much smaller than a GCM grid box (A. V. Korolev et al., 2003; Chylek & Borel, 2004; Field et al., 2004). By reducing the spatial overlap of ice and liquid condensate, this heterogeneity could limit WBF efficiency in the real atmosphere, and previous work has shown that accounting for heterogeneity can mitigate model biases in phase partitioning (Tan & Storelvmo, 2016;

84 Zhang et al., 2019; Huang et al., 2021). An important takeaway from this previous work  
85 is that there is no one-size-fits-all adjustment to WBF efficiency that improves model  
86 phase biases across the board: the sensitivity of phase biases to WBF efficiency varies  
87 with location, season, and temperature, and this variability presumably reflects differ-  
88 ent degrees of phase heterogeneity in the real world. Attempts to reduce model phase  
89 biases, if they are to be physically grounded, must therefore account not only for the ex-  
90 istence of phase heterogeneity but also for its spatial and temporal variability.

91 Understanding phase heterogeneity in the real atmosphere is a difficult problem  
92 because it occurs on scales ranging from microns to kilometers (A. V. Korolev et al., 2003;  
93 Atlas et al., 2021). Capturing this range of scales requires in situ aircraft observations,  
94 which typically have a measurement frequency of 1 Hz (every 100-200 m, depending on  
95 aircraft speed). Studies making use of the measurements have generally shown that a  
96 relatively small portion of 1-Hz observations within the mixed-phase temperature range  
97 contain both liquid and ice; most are single-phase or heavily dominated by one phase  
98 or the other (A. V. Korolev et al., 2003; Field et al., 2004; D’Alessandro et al., 2019; D’Alessandro  
99 et al., 2021; Zhang et al., 2019). For example, Zhang et al. (2019) analyzed data from  
100 the HIPPO aircraft campaign and found that only 13.4% of 1-Hz observations between  
101 -40-0°C were mixed-phase. Even when the data were smoothed by a 100-s ( $\sim$ 20-km) rolling  
102 average, only 25.8% were mixed-phase. On the whole, these aircraft studies suggest that  
103 mixed-phase conditions at the 100-m scale are relatively rare. This is not surprising given  
104 that mixtures of liquid and ice are thermodynamically unstable, which is what gives rise  
105 to the WBF process in the first place. Nevertheless, these observational assessments come  
106 with considerable uncertainty arising from imperfect phase classification algorithms and  
varying definitions of “mixed-phase”. Perhaps most importantly, aircraft observations  
are limited in number, and the generalizability of existing observations is unknown.

99 Spaceborne satellite observations are a largely untapped resource for studying cloud  
100 phase heterogeneity. Thompson et al. (2018) assessed cloud-top phase heterogeneity us-  
101 ing retrievals from the Hyperion spectrometer, but the spatial coverage of the observa-  
102 tions was sparse and included very few measurements of the mid-latitude oceans, where  
103 model phase biases are most severe. Moreover, the reliance of the spectrometer retrieval  
104 on reflected sunlight meant that observations were limited to daytime hours and only  
105 reflected conditions near cloud top. These limitations can be largely overcome by polar-  
106 orbiting satellites with active sensors, which offer near-global coverage over extended pe-

107 riods of time and can penetrate below cloud top until their signal is attenuated. While  
108 these satellites cannot capture the fine spatial scales observable by aircraft and Hype-  
109 rion, the aircraft observations discussed previously suggest that a resolution of a few hun-  
110 dred meters can capture a large portion of cloud phase variability. For these reasons, we  
111 believe active-sensing satellites are a promising avenue for understanding phase hetero-  
112 geneity on a global scale and improving its representation in models.

113 The goal of this work is to quantify cloud phase heterogeneity and its spatiotem-  
114 poral variability using spaceborne lidar measurements. The lidar observations are de-  
115 scribed in section 2. In section 3, we develop a metric that is used to characterize phase  
116 heterogeneity in the satellite record. Results are presented in section 4 and 5 and dis-  
117 cussed in section 6.

## 118 **2 Observational Data**

119 Observations of cloud phase were obtained from the Cloud-Aerosol Lidar with Or-  
120 thogonal Polarization (CALIOP) aboard the polar-orbiting CALIPSO satellite (Winker  
121 et al., 2009). The reasons for using CALIOP are its near-global coverage and its rela-  
122 tively high horizontal resolution: single-shot profiles of the atmosphere have a horizon-  
123 tal footprint of 90 m and are recorded every 333 m along the satellite’s path.

124 In the CALIOP retrievals used here (version 4), cloud phase is determined based  
125 on the layer-integrated attenuated backscatter and depolarization ratio (Hu et al., 2009;  
126 Avery et al., 2020). Each cloudy pixel is classified as liquid, randomly oriented ice, hor-  
127 izontally oriented ice, or unknown. Each phase determination is accompanied by a qual-  
128 ity indicator, which we use to eliminate low-confidence determinations. The lack of a mixed-  
129 phase classification is a clear limitation of the CALIOP phase retrievals, since mixed-  
130 phase conditions are known to occur on length scales much smaller than 333 m (Field  
131 et al., 2004; Atlas et al., 2021). Clouds identified as supercooled liquid may contain small  
132 amounts of ice that cannot be detected by spaceborne lidar because, in mixed-phase con-  
133 ditions, the number concentration of ice crystals is generally much lower than that of liq-  
134 uid droplets (Mace et al., 2021).

135 The cloud phase data used here are from CALIOP Level 2 Vertical Feature Mask  
136 data product (version 4.20; NASA/LARC/SD/ASDC, 2018b), which provides cloud phase  
137 retrievals at the single-shot resolution of 333 m up to an altitude of 8.2 km, above which

138 the resolution if coarsened due to bandwidth limitations. Because we wish to use the finest  
 139 resolution possible, we restrict our analysis to levels below 8.2 km. This is not an issue  
 140 for studying the mid- and high latitudes, where clouds above 8.2 km are almost entirely  
 141 ice (Cesana et al., 2015). We use all available data for the three-year period between 2009-  
 142 12-01 and 2012-11-30. This amounts to over 35 billion individual cloud observations, 83%  
 143 of which have medium- or high-quality phase determinations. Temperature data for the  
 144 same period are obtained from the CALIOP Level 2 Cloud Profile data product (version  
 145 4.20; NASA/LARC/SD/ASDC, 2018a), which provides temperature from the GEOS-  
 146 5 reanalysis interpolated onto the CALIPSO track with a horizontal resolution of 5 km  
 147 and a vertical resolution of 60 m. We further interpolate the temperature data onto the  
 148 single-shot grid of the cloud phase observations.

### 149 **3 Quantification of Phase Heterogeneity**

150 Previous work has quantified phase heterogeneity based on the frequency of switches  
 151 between liquid and ice along an aircraft flight track or on the horizontal extent of single-  
 152 phase patches within a cloud (Atlas et al., 2021; D’Alessandro et al., 2021). Here we use  
 153 a metric that is similar in nature but adjusted for use with CALIOP retrievals. We de-  
 154 fine the *interface density*  $I$  [ $\text{km}^{-1}$ ] as the number of interfaces between observations of  
 155 unlike phase per horizontal kilometer of cloud detected by CALIOP. To compute  $I$ , we  
 156 compare the phase of each cloud observation to the phase of the immediately adjacent  
 157 observations at the same vertical level. The boundary between two pixels is considered  
 158 to be a liquid-ice interface only if one of the pixels is liquid and the other is ice (either  
 159 randomly or horizontally oriented) and only if both phase determinations are of medium  
 160 or high confidence. Each cloud observation is assigned a value of 0, 1, or 2 equal to the  
 161 number of liquid-ice interfaces at its horizontal edges. We can then compute  $I$  for any  
 162 subset of observations as

$$I = \frac{(N_1/2 + N_2)}{N_c \cdot \Delta x} \quad (1)$$

163 where  $N_1$  and  $N_2$  are the number of cloud observations with one and two adjacent in-  
 164 terfaces, respectively, and  $N_c = N_0 + N_1 + N_2$  is the total number of cloud observa-  
 165 tions with medium- or high-confidence phase determinations.  $N_1$  is scaled by a factor  
 166 of 1/2 so that interfaces are not double-counted.  $\Delta x$  is the horizontal resolution of the  
 167 retrievals (333 m).

168 When  $l$  is large, cloud phase is more heterogeneous: single-phase cloud segments  
 169 are shorter in length and there is a greater contact area between liquid-only and ice-only  
 170 patches. Conversely, small  $l$  corresponds to large patches of uniform phase. While  $l$  can  
 171 be conceptualized as the inverse of the average length of a single-phase patch, we note  
 172 that the two quantities are not numerically equal because the edge of a cloud is not a  
 173 liquid-ice interface but nevertheless constitutes the end of a single-phase patch. The two  
 174 quantities are equal only in the limiting case of a cloud with infinite length.

Figure 1. Schematic illustrating the interface density metric,  $l$ , used to quantify cloud phase heterogeneity. Each box represents one single-shot lidar profile and its associated high-quality phase retrieval, with the number below indicating the number of liquid-ice interfaces adjacent to the box. Clouds transects A, B, and C all portray clouds that extend for 2-km along the satellite's track. A is single-phase liquid cloud while B and C are mixed-phase clouds with different degrees of heterogeneity.  $l$  is computed for each transect following Equation 1.

175 Figure 1 illustrates  $l$  for three schematic cloud transects of equal length. Transect  
 176 A, an all-liquid cloud with no phase interfaces, represents the most homogeneous possibility ( $l=0$ ). Transect C, a mixed-phase cloud in which liquid and ice alternate with  
 177 every observation, represents the most heterogeneous possibility. While  $l=2.5 \text{ km}^{-1}$   
 178 for transect C, we note that the theoretical maximum  $l$  is  $3 \text{ km}^{-1}$  ( $=1/\Delta x$ ), which corresponds to an infinitely long cloud with alternating phase retrievals. Transect B, which  
 179 shows a mixed-phase cloud with one liquid-ice interface, is a compromise between the  
 180 two extremes.  
 181  
 182

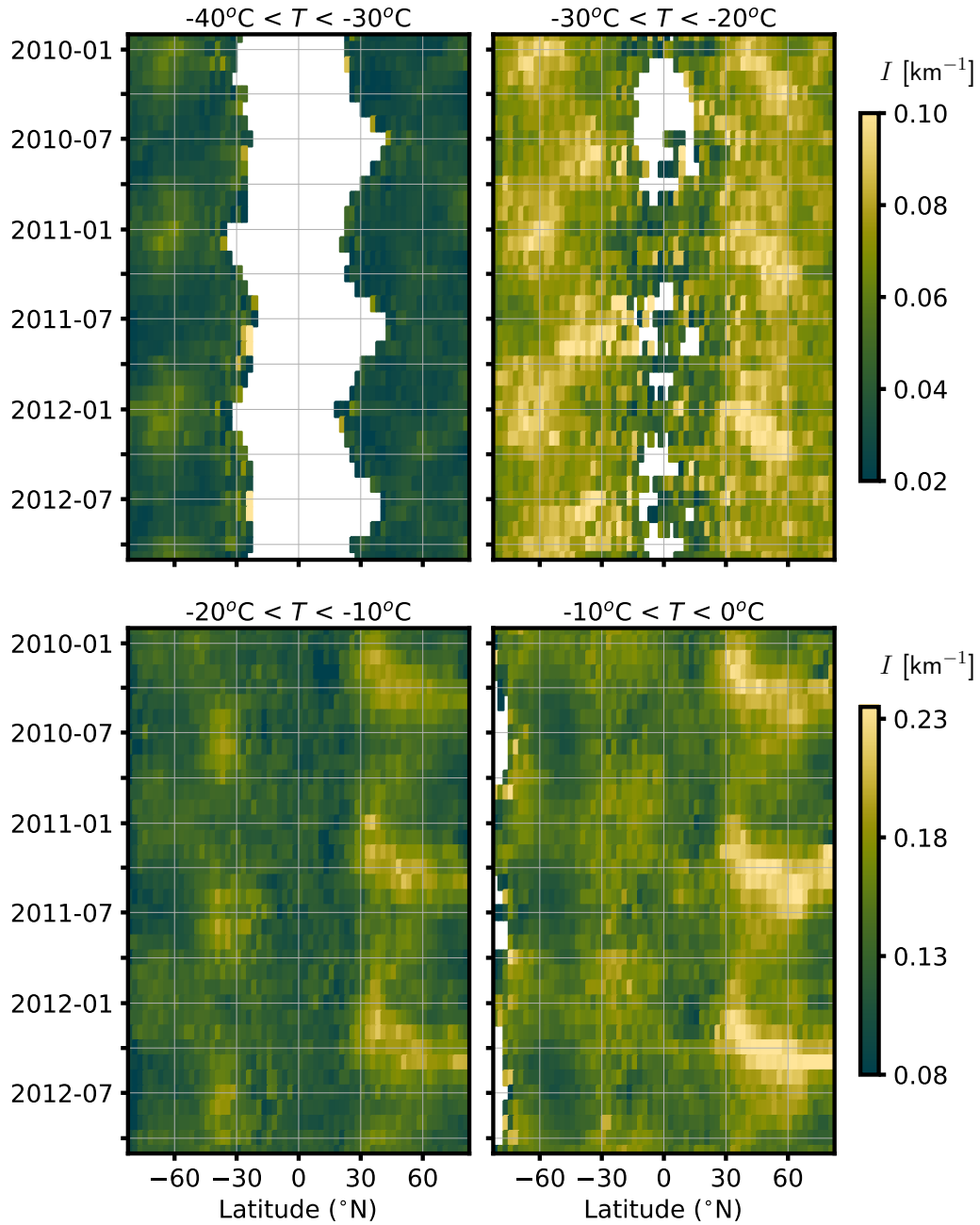


**Figure 3.** Zonal monthly mean  $I$  throughout the three-year study period for four different temperature brackets. Data are only shown for bins containing  $10^4$  or more cloud phase retrievals. The top two panels use a different color scale than the bottom two panels in order to highlight the variability within each temperature range.

256

The annual cycle of phase heterogeneity in the SH is similar in some respects to that in the NH but different in others. As in the NH, at  $30^{\circ}$ - $40^{\circ}$ S  $I$  is greatest during lo-

257

258 cal winter, when the storm track is more equatorward than at any other point in the year.  
259 Notably, this feature is only seen between  $-30^{\circ}$  and  $-10^{\circ}$ C and not in the warmest tem-  
260 perature bin. Unlike the NH, there is no clear progression of enhanced  $I$  towards the poles  
261 over the course of the spring. Poleward of  $50^{\circ}$ S,  $I$  is greatest during summer. Uncover-  
262 ing the shifts in cloud type that are responsible for these seasonal shifts in phase het-  
263 erogeneity may be a worthwhile endeavor but is beyond our scope here.

264 It is notable that  $I$  is relatively low over the Southern Ocean (SO) region ( $\sim 50$ -  
265  $70^{\circ}$ S) compared to similar latitudes in the NH. This is consistent with the fact that, in  
266 some models, biases in LCF and absorbed shortwave radiation are larger over the SO  
267 than in the extratropical NH (Trenberth & Fasullo, 2010; Tan et al., 2016; Kay et al.,  
268 2016). Lower  $I$  over the SO implies relatively little contact area between liquid and ice  
269 and thus a reduced potential for widespread WBF glaciation. The failure of models to  
270 account for subgrid phase heterogeneity would thus be expected to produce the largest  
271 LCF biases where  $I$  is low.

272 The seasonality in phase heterogeneity over the SO is also consistent with expecta-  
273 tions from previous modeling studies. Kay et al. (2016) found that SO phase parti-  
274 tioning biases in the CAM5 model were greatest between March and August (see their  
275 Figs. 9 and 10). Figure 3 shows that  $I$  at  $60^{\circ}$ S is lowest during this half of the year through-  
276 out the entire mixed-phase temperature range. These results underscore the need to in-  
277 incorporate seasonal variability into model representations of subgrid heterogeneity.

## 278 **6 Discussion**

279 The results shown here show that cloud phase heterogeneity has strong dependen-  
280 cies on temperature, latitude, and time of year. Even at fixed latitude and temperature,  
281  $I$  can vary by factor of  $\sim 2$  over the course of the year; such variability has important im-  
282 plications for WBF glaciation and should be accounted for in any model implementa-  
283 tion of subgrid phase heterogeneity. Figure 4 proposes one relatively simple way of ac-  
284 counting for this variability: mean  $I$  is computed for five zonal bands, four seasons, and  
285 four  $10^{\circ}$ C temperature ranges. While these bins are relatively coarse, they capture most  
286 of the variability in phase heterogeneity evident in Figure 3. The values shown in Fig-  
287 ure 4 are available in Data Set S2.

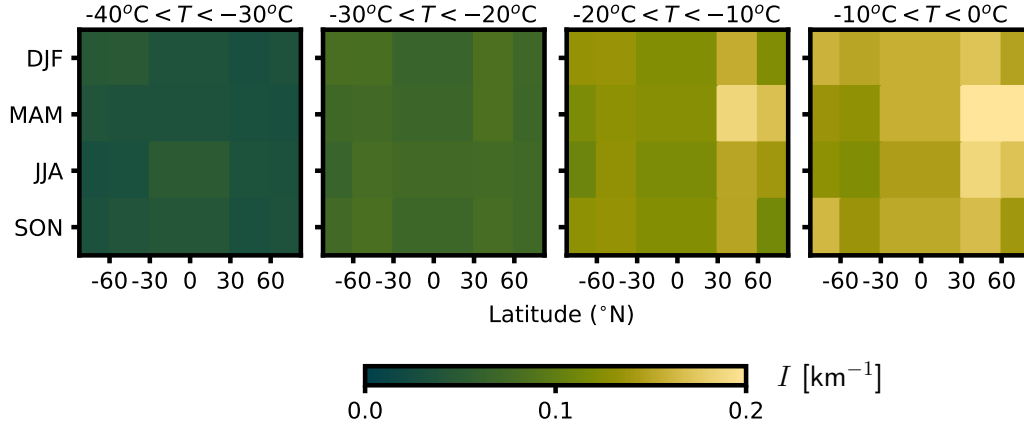


**Figure 4.** Zonally and seasonally averaged  $I$  for four different temperature brackets.

288 Future work will focus on how to meaningfully convert  $I$  to a scaling parameter that  
 289 can be used to adjust WBF efficiency in models. Such implementation must consider the  
 290 fact that  $I$  is a measure of liquid-ice interface density at a fixed vertical level along a one-  
 291 dimensional satellite track. Even if vertical phase heterogeneity is to be neglected,  $I$  must  
 292 still be generalized from one horizontal dimension to two. Implementations may vary from  
 293 model to model due to differences in grid type and WBF parameterizations, and for this  
 294 reason we leave the details of such implementation for future work.

295 The use of CALIOP to study phase heterogeneity has several sources of error in  
 296 addition to the limitation of horizontal resolution discussed in section 1. About 17% of  
 297 the cloud observations in our study period lacked a high-quality phase determination and  
 298 were not included in our analysis. Thus, the number of liquid-ice interfaces identified us-  
 299 ing our methodology is almost certainly an underestimate, not to mention the fact that  
 300 some of the excluded observations are likely mixed-phase. Another potential source of  
 301 bias is the fact that the lidar signal attenuates at an optical depth of  $\sim 5$  (Winker et al.,  
 302 2009), which means that our results are skewed to represent conditions near cloud top  
 303 for optically thick clouds, such as the low marine clouds common over the Southern Ocean.  
 304 This bias would only affect our results if there is significant vertical variation in cloud  
 305 phase heterogeneity. Lastly, we draw attention to the source of error discussed in Mace  
 306 et al. (2021), who demonstrated the difficulty of observing mixed-phase clouds using space-  
 307 borne lidar. In particular, they documented the presence of low clouds over the South-  
 308 ern Ocean that are mixed-phase but appear to spaceborne lidar as supercooled liquid

309 because the layer scattering characteristics are heavily dominated by liquid droplets. The  
 310 inability of spaceborne lidar to identify the presence of ice in such clouds is an inherent  
 311 limitation of our methodology.

312 This paper presents, to our knowledge, the first comprehensive, global assessment  
 313 of cloud phase heterogeneity using spaceborne satellites. Such an assessment is valuable  
 314 because it strikes a balance between horizontal resolution and spatiotemporal coverage.  
 315 While spaceborne lidar cannot be used to study phase heterogeneity on the scale of in-  
 316 dividual cloud particles, our results show that it is capable of capturing differences in  
 317 phase heterogeneity on scales much smaller than a GCM grid box. In this way, it offers  
 318 a useful complement to *in situ* aircraft observations and a good opportunity to improve  
 319 model representations of cloud phase.

## 320 7 Open Research

321 The CAIOP retrievals used in this study (NASA/LARC/SD/ASDC, 2018a, 2018b)  
 322 are publicly available at <https://search.earthdata.nasa.gov>. Phase heterogeneity statis-  
 323 tics are provided in Data Set S1.

## 324 Acknowledgments

325 This work was supported by the European Research Council (ERC) through Grant StG  
 326 758005.

## 327 References

- 328 Atlas, R., Mohrmann, J., Finlon, J., Lu, J., Hsiao, I., Wood, R., & Diao, M. (2021,  
 329 November). The University of Washington Ice–Liquid Discriminator (UWILD)  
 330 improves single-particle phase classifications of hydrometeors within Southern  
 331 Ocean clouds using machine learning. *Atmospheric Measurement Techniques*,  
 332 *14*(11), 7079–7101. doi: 10.5194/amt-14-7079-2021
- 333 Avery, M. A., Ryan, R. A., Getzewich, B. J., Vaughan, M. A., Winker, D. M., Hu,  
 334 Y., . . . Verhappen, C. A. (2020, August). CALIOP V4 cloud thermodynamic  
 335 phase assignment and the impact of near-nadir viewing angles. *Atmospheric*  
 336 *Measurement Techniques*, *13*(8), 4539–4563. doi: 10.5194/amt-13-4539-2020
- 337 Cesana, G., Chepfer, H., Winker, D., Getzewich, B., Cai, X., Jourdan, O., . . .  
 338 Reverdy, M. (2016). Using in situ airborne measurements to evaluate three

- 339 cloud phase products derived from CALIPSO. *Journal of Geophysical Re-*  
340 *search: Atmospheres*, 121(10), 5788–5808. doi: 10.1002/2015JD024334
- 341 Cesana, G., Waliser, D. E., Jiang, X., & Li, J.-L. F. (2015). Multimodel eval-  
342 uation of cloud phase transition using satellite and reanalysis data. *Jour-*  
343 *nal of Geophysical Research: Atmospheres*, 120(15), 7871–7892. doi:  
344 10.1002/2014JD022932
- 345 Choi, Y.-S., Ho, C.-H., Park, C.-E., Storelvmo, T., & Tan, I. (2014). Influence of  
346 cloud phase composition on climate feedbacks. *Journal of Geophysical Re-*  
347 *search: Atmospheres*, 119(7), 3687–3700. doi: 10.1002/2013JD020582
- 348 Chylek, P., & Borel, C. (2004). Mixed phase cloud water/ice structure from high  
349 spatial resolution satellite data. *Geophysical Research Letters*, 31(14). doi: 10  
350 .1029/2004GL020428
- 351 D’Alessandro, J. J., McFarquhar, G. M., Wu, W., Stith, J. L., Jensen, J. B., &  
352 Rauber, R. M. (2021). Characterizing the Occurrence and Spatial Heterogene-  
353 ity of Liquid, Ice, and Mixed Phase Low-Level Clouds Over the Southern  
354 Ocean Using in Situ Observations Acquired During SOCRATES. *Jour-*  
355 *nal of Geophysical Research: Atmospheres*, 126(11), e2020JD034482. doi:  
356 10.1029/2020JD034482
- 357 D’Alessandro, J. J., Diao, M., Wu, C., Liu, X., Jensen, J. B., & Stephens, B. B.  
358 (2019, May). Cloud Phase and Relative Humidity Distributions over  
359 the Southern Ocean in Austral Summer Based on In Situ Observations  
360 and CAM5 Simulations. *Journal of Climate*, 32(10), 2781–2805. doi:  
361 10.1175/JCLI-D-18-0232.1
- 362 Field, P. R., Hogan, R. J., Brown, P. R. A., Illingworth, A. J., Choulaton, T. W.,  
363 Kaye, P. H., . . . Greenaway, R. (2004). Simultaneous radar and aircraft ob-  
364 servations of mixed-phase cloud at the 100 m scale. *Quarterly Journal of the*  
365 *Royal Meteorological Society*, 130(600), 1877–1904. doi: 10.1256/qj.03.102
- 366 Frey, W. R., & Kay, J. E. (2018, April). The influence of extratropical cloud phase  
367 and amount feedbacks on climate sensitivity. *Climate Dynamics*, 50(7), 3097–  
368 3116. doi: 10.1007/s00382-017-3796-5
- 369 Hoskins, B. J., & Hodges, K. I. (2019, March). The Annual Cycle of Northern  
370 Hemisphere Storm Tracks. Part II: Regional Detail. *Journal of Climate*, 32(6),  
371 1761–1775. doi: 10.1175/JCLI-D-17-0871.1

- 372 Hu, Y., Winker, D., Vaughan, M., Lin, B., Omar, A., Trepte, C., . . . Kuehn, R.  
373 (2009, November). CALIPSO/CALIOP Cloud Phase Discrimination Algo-  
374 rithm. *Journal of Atmospheric and Oceanic Technology*, *26*(11), 2293–2309.  
375 doi: 10.1175/2009JTECHA1280.1
- 376 Huang, Y., Dong, X., Kay, J. E., Xi, B., & McIlhattan, E. A. (2021, May). The  
377 climate response to increased cloud liquid water over the Arctic in CESM1: a  
378 sensitivity study of Wegener–Bergeron–Findeisen process. *Climate Dynamics*,  
379 *56*(9), 3373–3394. doi: 10.1007/s00382-021-05648-5
- 380 Kay, J. E., Bourdages, L., Miller, N. B., Morrison, A., Yettella, V., Chepfer, H.,  
381 & Eaton, B. (2016). Evaluating and improving cloud phase in the Com-  
382 munity Atmosphere Model version 5 using spaceborne lidar observations.  
383 *Journal of Geophysical Research: Atmospheres*, *121*(8), 4162–4176. doi:  
384 10.1002/2015JD024699
- 385 Komurcu, M., Storelvmo, T., Tan, I., Lohmann, U., Yun, Y., Penner, J. E., . . .  
386 Takemura, T. (2014). Intercomparison of the cloud water phase among global  
387 climate models. *Journal of Geophysical Research: Atmospheres*, *119*(6), 3372–  
388 3400. doi: 10.1002/2013JD021119
- 389 Korolev, A., McFarquhar, G., Field, P. R., Franklin, C., Lawson, P., Wang, Z.,  
390 . . . Wendisch, M. (2017, January). Mixed-Phase Clouds: Progress and  
391 Challenges. *Meteorological Monographs*, *58*(1), 5.1–5.50. doi: 10.1175/  
392 AMSMONOGRAPHS-D-17-0001.1
- 393 Korolev, A. V., Isaac, G. A., Cober, S. G., Strapp, J. W., & Hallett, J. (2003). Mi-  
394 crophysical characterization of mixed-phase clouds. *Quarterly Journal of the*  
395 *Royal Meteorological Society*, *129*(587), 39–65. doi: 10.1256/qj.01.204
- 396 Mace, G. G., Protat, A., & Benson, S. (2021). Mixed-Phase Clouds Over the South-  
397 ern Ocean as Observed From Satellite and Surface Based Lidar and Radar.  
398 *Journal of Geophysical Research: Atmospheres*, *126*(16), e2021JD034569. doi:  
399 10.1029/2021JD034569
- 400 McIlhattan, E. A., L’Ecuyer, T. S., & Miller, N. B. (2017, June). Observa-  
401 tional Evidence Linking Arctic Supercooled Liquid Cloud Biases in CESM  
402 to Snowfall Processes. *Journal of Climate*, *30*(12), 4477–4495. doi:  
403 10.1175/JCLI-D-16-0666.1
- 404 Mitchell, J. F. B., Senior, C. A., & Ingram, W. J. (1989, September). C02

- 405 and climate: a missing feedback? *Nature*, *341*(6238), 132–134. doi:  
406 10.1038/341132a0
- 407 NASA/LARC/SD/ASDC. (2018a, October). *CALIPSO Lidar Level 2 Cloud Pro-*  
408 *file, V4-20*. NASA Langley Atmospheric Science Data Center DAAC. Re-  
409 trieved from [https://doi.org/10.5067/CALIOP/CALIPSO/LID\\_L2\\_05KMCPR0](https://doi.org/10.5067/CALIOP/CALIPSO/LID_L2_05KMCPR0)  
410 *-STANDARD-V4-20*
- 411 NASA/LARC/SD/ASDC. (2018b, October). *CALIPSO Lidar Level 2 Vertical Fea-*  
412 *ture Mask (VFM), V4-20*. NASA Langley Atmospheric Science Data Center  
413 DAAC. Retrieved from [https://doi.org/10.5067/CALIOP/CALIPSO/LID\\_L2](https://doi.org/10.5067/CALIOP/CALIPSO/LID_L2_VFM-STANDARD-V4-20)  
414 *\_VFM-STANDARD-V4-20*
- 415 Storelvmo, T., & Tan, I. (2015). The Wegener-Bergeron-Findeisen process - Its  
416 discovery and vital importance for weather and climate. *Meteorologische*  
417 *Zeitschrift*, *24*(4), 455–461. doi: 10.1127/METZ/2015/0626
- 418 Storelvmo, T., Tan, I., & Korolev, A. V. (2015, December). Cloud Phase Changes  
419 Induced by CO<sub>2</sub> Warming—a Powerful yet Poorly Constrained Cloud-  
420 Climate Feedback. *Current Climate Change Reports*, *1*(4), 288–296. doi:  
421 10.1007/s40641-015-0026-2
- 422 Tan, I., & Storelvmo, T. (2016, February). Sensitivity Study on the Influence  
423 of Cloud Microphysical Parameters on Mixed-Phase Cloud Thermodynamic  
424 Phase Partitioning in CAM5. *Journal of the Atmospheric Sciences*, *73*(2),  
425 709–728. doi: 10.1175/JAS-D-15-0152.1
- 426 Tan, I., Storelvmo, T., & Zelinka, M. D. (2016, April). Observational constraints on  
427 mixed-phase clouds imply higher climate sensitivity. *Science*, *352*(6282), 224–  
428 227. doi: 10.1126/science.aad5300
- 429 Thompson, D. R., Kahn, B. H., Green, R. O., Chien, S. A., Middleton, E. M., &  
430 Tran, D. Q. (2018, February). Global spectroscopic survey of cloud thermody-  
431 namic phase at high spatial resolution, 2005–2015. *Atmospheric Measurement*  
432 *Techniques*, *11*(2), 1019–1030. doi: 10.5194/amt-11-1019-2018
- 433 Trenberth, K. E., & Fasullo, J. T. (2010, January). Simulation of Present-Day and  
434 Twenty-First-Century Energy Budgets of the Southern Oceans. *Journal of Cli-*  
435 *mate*, *23*(2), 440–454. doi: 10.1175/2009JCLI3152.1
- 436 Tsushima, Y., Emori, S., Ogura, T., Kimoto, M., Webb, M. J., Williams, K. D., ...  
437 Andronova, N. (2006, August). Importance of the mixed-phase cloud distri-

- 438           bution in the control climate for assessing the response of clouds to carbon  
439           dioxide increase: a multi-model study. *Climate Dynamics*, *27*(2), 113–126. doi:  
440           10.1007/s00382-006-0127-7
- 441 Winker, D. M., Vaughan, M. A., Omar, A., Hu, Y., Powell, K. A., Liu, Z., ...  
442           Young, S. A.     (2009, November).     Overview of the CALIPSO Mission and  
443           CALIOP Data Processing Algorithms.     *Journal of Atmospheric and Oceanic*  
444           *Technology*, *26*(11), 2310–2323. doi: 10.1175/2009JTECHA1281.1
- 445 Zelinka, M. D., Myers, T. A., McCoy, D. T., Po-Chedley, S., Caldwell, P. M.,  
446           Ceppi, P., ... Taylor, K. E.     (2020, January).     Causes of Higher Climate  
447           Sensitivity in CMIP6 Models.     *Geophysical Research Letters*, *47*(1).     doi:  
448           10.1029/2019GL085782
- 449 Zhang, M., Liu, X., Diao, M., D’Alessandro, J. J., Wang, Y., Wu, C., ... Xie, S.  
450           (2019).     Impacts of Representing Heterogeneous Distribution of Cloud Liq-  
451           uid and Ice on Phase Partitioning of Arctic Mixed-Phase Clouds with NCAR  
452           CAM5. *Journal of Geophysical Research: Atmospheres*, *124*(23), 13071–13090.  
453           doi: 10.1029/2019JD030502